Opto-Electronics Review

journal homepage: https://journals.pan.pl/opelre

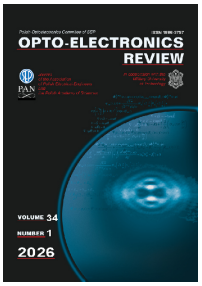

NiO-ZnO heterostructure with photocatalytic activity

Izabela Stępińska[1*], Joanna Rymarczyk[1], Mirosław Kozłowski[1], Ryszard Diduszko[2]

[1] Łukasiewicz Research Network – Tele and Radio Research Institute, ul. Ratuszowa 11, 03-450 Warsaw, Poland
[2] Institute of Physics, Polish Academy of Sciences, Al. Lotników 32/46, 02-668 Warsaw, Poland

Article info

Article history:
Received 30 Oct. 2025
Received in revised form 19 Dec. 2025
Accepted 29 Dec. 2025
Available on-line 06 Feb. 2026

Keywords:
nickel oxide;
zinc oxide;
heterostructure;
photocatalysis.

Abstract

The NiO-ZnO heterostructures were fabricated using a combination of physical vapour deposition and thermal oxidation techniques. Thin films of nickel and zinc were sequentially deposited onto non-conductive substrates and subsequently oxidised to form nanostructured p–n junctions. The influence of thermal oxidation parameters on the structural, morphological, and optical properties of the resulting heterostructures was thoroughly investigated using scanning electron microscopy, high-resolution transmission microscopy, X-ray diffraction, and UV-Vis spectroscopy. The heterostructures exhibited a strong UV absorption and a band gap of 3.29 eV. Photocatalytic activity was evaluated using an aqueous solution of methylene blue under UV irradiation. The NiO-ZnO films achieved a degradation efficiency of 93% after 540 min, confirming their potential for photocatalytic water treatment applications. These preliminary findings demonstrate that even thin-film configurations with limited catalyst mass can be promising in degrading organic pollutants.

1. Introduction

The constant growth of industry causes alarming environmental pollution. Alternative methods for treating the large volumes of wastewater containing chemicals such as pesticides, pharmaceuticals, dyes, and others are required. These methods need to be sustainable and respectful of the natural environment. Advanced oxidation processes (AOPs) have been widely used for the disinfection of drinking water, removal of organic pollutants, and wastewater treatment [1]. These processes encompass many chemical methods, often enhanced with light or electrical activation. Regardless of the method, the main mechanism is the generation of highly reactive oxygen radicals, including hydroxyl radicals (·OH) and oxygen anion (O^{2-}), which effectively break down organic pollutants through redox reactions. The most recognisable AOPs methods are (i) ozonation/ultraviolet (UV) light, (ii) Fenton processes, (iii) photocatalysis, (iv) electrochemical oxidation, (v) cavitation processes. Based on the literature review, it can be concluded that photocatalysis is perceived as the process of the future. It is mainly used for water and air purification, as well as in the energy industry for hydrogen production, offering a pure and favourable approach [2–4]. According to IUPAC, the definition of photocatalysis is "*change in the rate of a chemical reaction or its initiation under the action of ultraviolet, visible, or infrared radiation in the presence of a substance – the photocatalyst – that absorbs light and is involved in the chemical transformation of the reaction partners*" [5]. Most photocatalysts are semiconducting materials that generate electron-hole pairs upon exposure to light. Excited electrons are the reductive agent, and holes are the oxidative agent. When reacting with an organic molecule, they degrade or mineralise it to a harmless substance.

Fujishima's and Honda's studies are considered pioneering findings in the field of photocatalysis involving the TiO_2 n-type semiconductor [6]. The researchers demonstrated the possibility of water splitting via a photoelectrochemical process. A TiO_2 electrode was used in conjunction with a platinum electrode via an external circuit. When the TiO_2 electrode was irradiated with UV light, the current flowed through the circuit. The result of this process was the decomposition of water to hydrogen and oxygen. This work initiated numerous studies on semiconductor photocatalysis, in which TiO_2 remained the main focus.

TiO_2 has become one of the most well-known photocatalysts [7–10] due to its undoubted advantages such as wide band gap, non-toxicity, chemical stability, and high reactivity. However, TiO_2 also has certain limitations, such as rapid recombination and limited light absorption range [11]. Therefore, researchers have begun to explore other semiconductors with better photocatalytic properties.

*Corresponding author at: izabela.stepinska@itr.lukasiewicz.gov.pl

https://doi.org/10.24425/opelre.2026.157820
1896-3757/ Association of Polish Electrical Engineers (SEP) and Polish Academic of Sciences (PAS). Published by PAS

The most common are metal oxides, ZnO [12–14], ZrO [15], Fe_2O_3 [16], WO_3 [17], CeO_2 [18], and V_2O_5 [19], as well as sulphides ZnS [20], WS_2 [21], and CdS [22].

The efficiency of photocatalysts depends primarily on the semiconductor properties. The materials mentioned above have band gaps greater than 3 eV; consequently, only UV light can activate them. Moreover, rapid recombination of electron-hole pairs significantly reduces the process yield. Thus, numerous studies have focused on expanding the optical absorption into the visible spectrum and effectively separating charge carriers in single semiconductor photocatalysts to slow recombination [23–25]. This can be achieved by incorporating metal or non-metal dopants [26, 27], formatting new energy states [28], and coupling with other semiconductors.

By coupling two semiconductors with different band structures, a heterojunction can be formed that promotes charge separation via the internal electric field at the interface. Additionally, nanosized photocatalysts also exhibit greater photocatalytic activity than bulk materials [29–31]. Quantum effects and the formation of surface states in nanostructures such as nanoparticles, nanowires, or thin films can lead to a discretisation of energy levels, resulting in an increased energy band gap compared to their bulk counterparts. Among various systems, NiO-ZnO heterostructures have attracted considerable attention due to their complementary properties.

Nanostructured NiO is a p-type semiconductor, while ZnO is an n-type semiconductor. Both materials exhibit wide band gaps, ranging from 3.6 to 4.0 eV for NiO and 3.3 to 3.7 eV for ZnO [32, 33], leading to strong UV absorption and minimal response to visible light. Coupling thin films of NiO and ZnO forms a heterostructure that combines the unique properties of both semiconductors. The valence band of NiO is higher than that of ZnO, while the conduction band of ZnO is lower than that of NiO [34]. This creates a potential barrier that promotes the separation of charge carriers under UV irradiation. The probability of electron–hole recombination is reduced by this effective charge separation, which is beneficial for photocatalytic processes. The resulting charge carriers interact with water and oxygen molecules, generating reactive oxygen species that degrade organic pollutants [35]. Moreover, the wide band gap of the NiO-ZnO junction provides excellent thermal and chemical stability. Numerous literature reports have investigated the photocatalytic properties of ZnO and NiO in a heterostructure form. Gasmi *et al*. [36] reported that ZnO-NiO heterojunction thin films synthesised via a sol–gel dip-coating method exhibited outstanding photocatalytic activity, achieving 96.73% methylene blue (MB) degradation under sunlight, significantly surpassing pristine ZnO and NiO. This enhancement was attributed to efficient charge separation at the p–n junction, reactive oxygen species generation, and improved photodetector performance, with high responsivity and detectivity. The ZnO/NiO nanocomposite was employed for the photodegradation of methylene orange [37]. The nanocomposite was prepared via the hydrothermal method using zinc acetate and nickel nitrate for forming nanoparticles. The authors reported a maximum degradation efficiency of 76% at 180 min. In another study [38], the ZnO-NiO nanoparticles complex was added to reduced graphene oxide, which resulted in 90.24% MB degradation after 90 min. The results demonstrated significantly greater photocatalytic activity than the individual components.

In addition to photocatalytic applications, ZnO-based materials have been extensively investigated for UV photodetectors due to their wide band gap and strong absorption in the UV spectral range. Various ZnO nanostructures and heterostructures, including p–n junction systems such as ZnO-NiO, have been reported to exhibit high UV responsivity and good signal-to-noise characteristics [39, 40]. In particular, the formation of heterojunctions has been shown to enhance charge separation and suppress recombination, which are crucial for both optoelectronic and photocatalytic functionalities. Although the present work does not focus on UV photodetection, it is worth emphasising the versatility of ZnO-based heterostructures and the fundamental role of UV-induced charge-transfer mechanisms, which are also directly related to photocatalytic performance.

In this work, the structural and optical properties of the NiO-ZnO heterostructures were investigated. The photocatalytic performance of the obtained films was evaluated through the degradation of MB under UV irradiation.

2. Materials and methods

2.1. Preparation of NiO-ZnO heterostructure

NiO-ZnO heterostructures were obtained by combining physical vapour deposition and thermal oxidation techniques. First, a thin Ni film was deposited on the non-conductive substrates (quartz plate 2.1 × 0.8 × 0.1 cm) and subsequently annealed in air to form an NiO nanostructure. Afterward, a Zn thin film was deposited, followed by another annealing step. The film thicknesses were 50 nm for Ni and 100 nm for Zn.

Annealing was performed at 600 °C for 60 min for the Ni film and at 500 °C for 60 min for the Zn film. As a result, a two-thin-film NiO-ZnO system was obtained.

2.2. Characterisation methods

Structural characterisation of the obtained samples was performed using a Jeol JSM-7600 scanning electron microscopy (SEM), X-ray diffraction (XRD), and F200X transmission electron microscopy (TEM) equipped with an energy dispersive X-ray spectroscope – EDS by Bruker. The optical properties of the NiO-ZnO heterostructure were investigated using UV-Vis spectrophotometer (Evolution 300, Thermo Scientific). The photodegradation of a 5 mg/L MB, as a model wastewater pollutant, was investigated under both UV-A ($\lambda = 366$ nm) and UV-C ($\lambda = 254$ nm) irradiation (Herolab, HL, 4W). The photocatalytic activity of the NiO-ZnO heterostructure was measured by monitoring the absorbance of MB every 60 min.

3. Results and discussion

3.1. Structural properties

SEM, TEM, and XRD analyses of pure NiO and ZnO, which constitute the components of the heterostructure, are presented in Fig. 1 and Fig. 2. A densely packed granular morphology composed of uniformly distributed nanograins

of the NiO film is revealed in the SEM image [Fig. 1(a)]. The surface appears continuous and compact, with well-defined grain boundaries and negligible cracks, likely due to stress. The grain size is relatively homogenous and typically in the range of several to tens of nanometers, forming a closely interconnected network. The compact structure of NiO is expected to accelerate charge transport and stability, which is desirable in the photocatalysis process.

The typical HRTEM image of NiO nanograin [Figs. 1(b) and (c)] shows the lattice fringes with an interplanar spacing of 0.24 nm, and it is attributed to the (111) plane. The angle between the planes was measured to be 70.5°, characteristic of the cubic structure. The electron diffraction pattern [Fig. 1(e)] shows a set of concentric rings composed of numerous fine and sharp diffraction spots. This indicates a polycrystalline structure consisting of well-crystalised nanocrystals with random orientation. Each ring corresponds to a specific crystallographic plane. The XRD diffractogram of the NiO film is shown in Fig. 1(d). The sharp peaks at $2\theta \approx 37.25°$, 43.24°, and 62.85° correspond to the (111), (200), and (220) planes of a face-centered cubic (FCC), according to the JCPDS database (card no. 47-1049).

The SEM image [Fig. 2(a)] of a ZnO thin film reveals densely packed nanograins, which homogenously cover the surface. The grains exhibit a hexagonal or irregular shape typical of the wurtzite structure, consistent with the XRD results. Compared to the NiO film, the ZnO surface is slightly rougher. The average grain size is from tens to hundreds of nanometers, and they tend to agglomerate.

An interplanar spacing measured in the HRTEM image [Figs. 2(b) and (c)], were 0.28 nm and 0.25 nm, which correspond to the (100) and (101) planes of the hexagonal ZnO structure. These values are in good agreement with the standard patterns (ICDD card no. 01-070-2551). These results are supported by the XRD studies presented in Fig. 2(d). Well-defined peaks at 31.82°, 34.52°, 36.21°,

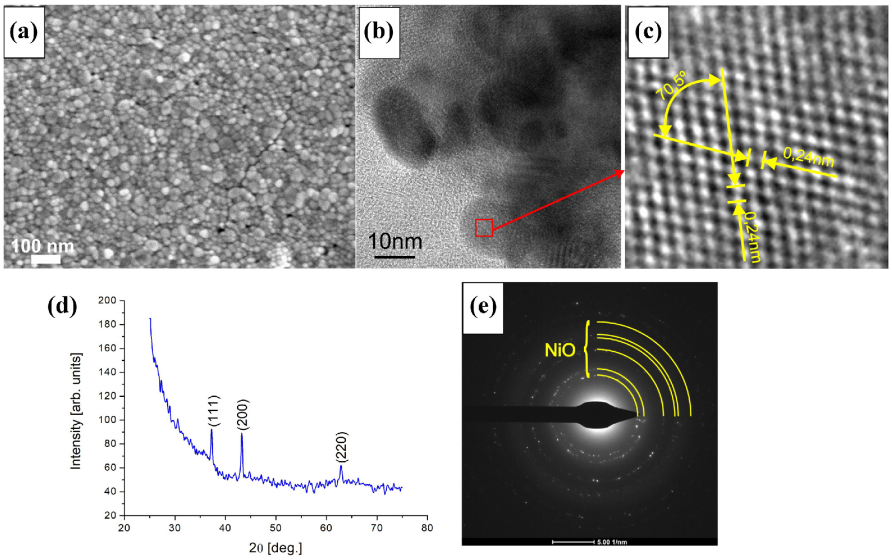

Fig. 1. (a) SEM image of NiO thin-film surface, (b) and (c) TEM images, (d) XRD pattern, (e) electron diffraction pattern of the NiO thin film.

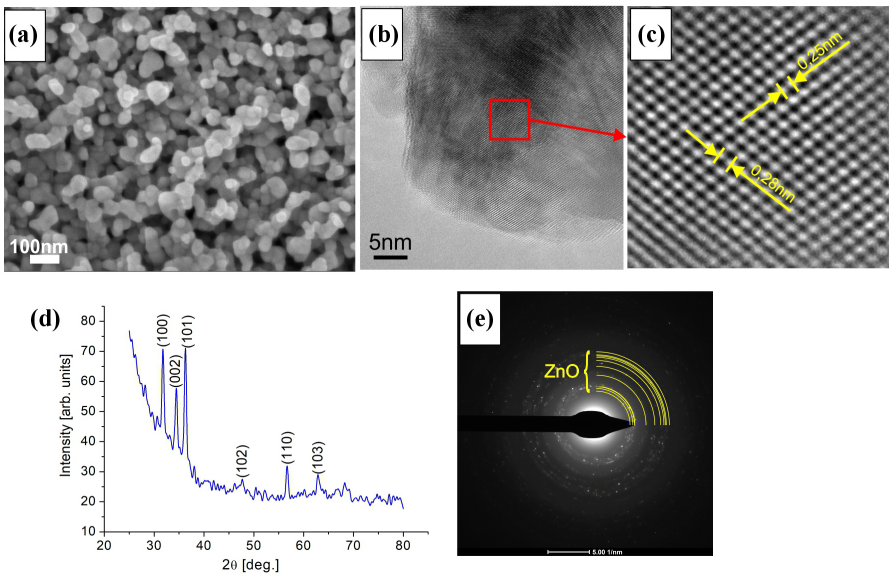

Fig. 2. (a) SEM image of ZnO thin-film surface, (b) and (c) TEM images, (d) XRD pattern, (e) electron diffraction pattern of the ZnO thin film.

56.75°, 62.84°, correspond to the (100), (002), (101), (102), (110), and (103) planes of the wurtzite ZnO structure, respectively. The electron diffraction pattern of ZnO [Fig. 2(e)] reveals discrete spots along the rings, confirming the high crystallinity and relatively large grain size of the crystallites.In the heterostructure, the ZnO film was deposited on top of the NiO film, forming the upper surface, so there is no difference in the SEM imaging topography between the NiO-ZnO and the ZnO samples.

Figure 3 presents the results of studies from different detectors used in TEM. Figure 3(a) is an image from a high angle annular dark field (HAADF) detector and provides Z-contrast information, highlighting compositional variations associated with differences in the atomic number of the constituent elements. Figures 3(b) and (c) show the distribution of chemical elements in the tested material: Ni, Zn, and O.

3.2. *Optical properties*

Figures 4(a) and 5(b) show the UV-Vis absorption spectra for NiO and ZnO thin films, respectively. The spectrum of NiO shows an absorption peak at ~290 nm, indicating the energy band gap of the obtained NiO film. Similarly, for the ZnO film, the absorbance intensity peak was observed at ~360 nm and may be ascribed as a near-band edge absorption. This shows that both NiO and ZnO films behave as semiconductor materials with an absorption edge in the UV region and are insensitive to visible light. The well-known Tauc's equation (1) allows to determine the value of the energy band gap (E_g) for NiO and ZnO:

$$(\alpha h\nu)^{1/n} = B\left(h\nu - E_g\right). \tag{1}$$

Here, α is the coefficient dependent on absorption, h is the Planck's constant, ν is the photon frequency, and B is the proportionality constant, n denotes the transition type (1/2 for indirect and 2 for direct transitions). Since NiO is an indirect semiconductor, $n = 1/2$, while ZnO, being a direct band gap material, uses $n = 2$.

Based on Tauc's diagram shown in Fig. 3(b), the value of a band gap for NiO was estimated as 3.52 eV and for ZnO $E_g = 3.26$ eV. There are many studies on the optical band gap of these materials. For example, Patil and Kadam [41] measured the energy gap in the range of 3.4–3.58 eV depending on thickness. In another study [42], the effect of technological parameters of the NiO layer preparation on the band gap was investigated, and it was found that E_g ranged from 3.60 to 3.80 eV depending on the annealing time.

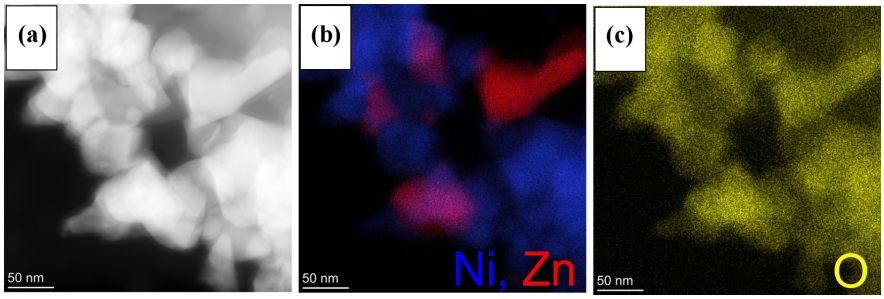

Fig. 3. TEM images of a fragment of NiO-ZnO heterostructure: (a) material contrast in the HAADF mode, (b) distribution of Ni and Zn, and (c) O in the EDS mode.

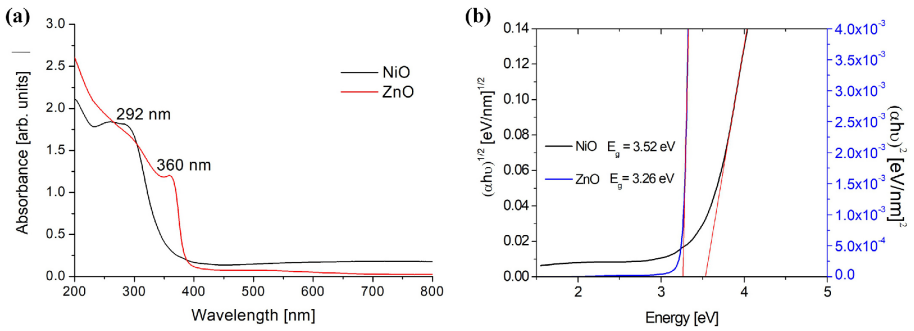

Fig. 4. (a) UV-Vis absorption spectra and (b) Tauc's plots for NiO and ZnO thin films.

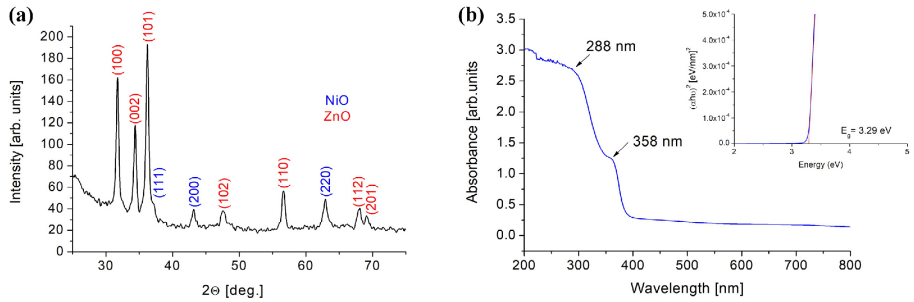

Fig. 5. (a) XRD spectrum and (b) UV-Vis spectrum of the NiO-ZnO heterostructure with Tauc's plot.

The calculated result of $E_g = 3.26$ eV for ZnO agrees with the literature reports regarding the energy gap value for thin ZnO films, 3.22–3.26 in [43] or 3.13–4.06 [44], for example.

The UV-Vis absorption spectrum of the NiO-ZnO heterostructure [Fig. 5(b)] exhibits two distinct absorption edges. The first absorption feature around 288 nm can be attributed to the NiO, while the second absorption edge near 360 nm is associated with the ZnO film. The presence of the metal oxide phases was confirmed by an XRD analysis. On the XRD spectrum [Fig. 5(a)] of the heterostructure, sharp peaks, similar to pure ZnO and pure NiO, are observed. Optical band gaps obtained from Tauc's analysis suggest that the heterostructure optical response is dominated by ZnO, while NiO contributes slighter and is disturbed by the interfacial effects at the NiO-ZnO interface. The band gap of the heterostructure was estimated to be 3.29 eV.

It should be noted that the energy band gap is affected by many factors, including film thickness, synthesis method and its parameters, and internal stresses within the film. Variations in deposition techniques, annealing conditions, and microstructural features such as grain size, crystallinity, and defect concentration can lead to noticeable shifts in the optical band gap.

3.3. *Photocatalytic activity*

Figure 6(c) shows the photocatalytic activity of the NiO-ZnO heterostructure along with a comparison with pure NiO and ZnO [Figs. 6(a) and (b)]. It is visible that NiO-ZnO has much better photocatalytic properties than pure NiO [Fig. 6(d)].

The degradation efficiency of MB (D) was determined using the following relation:

$$D = \frac{A_0 - A}{A_0} \cdot 100\%, \tag{2}$$

where A_0 and A correspond to the initial and time-dependent absorbance values of the MB solution, respectively. After 540 min of irradiation, the maximum degradation levels reached 93%, 79%, and 15% for the NiO-ZnO heterostructure, ZnO, and NiO samples, respectively [Fig. 7(a)].

To evaluate the reaction kinetics and rate constant, the natural logarithm of the concentration ratio $\ln(C_0/C)$ was plotted as a function of irradiation time, as shown in Fig. 7(b). Here, C_0 and C denote the initial and the momentary MB concentrations, respectively. The resulting linear relationship confirms that the photocatalytic

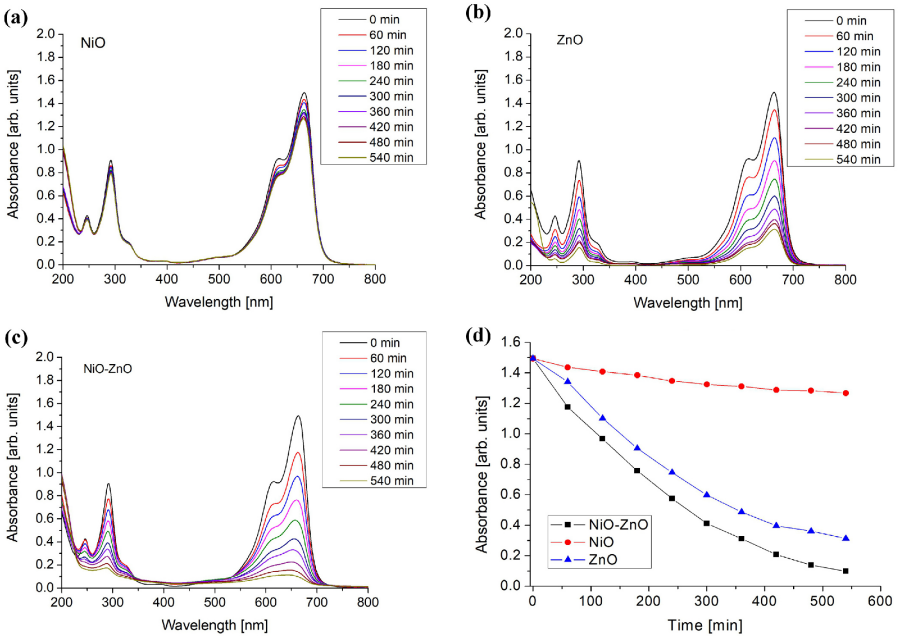

Fig. 6. UV-Vis spectra showing decomposition of the MB solution as a function of time with photocatalyst: (a) NiO, (b) ZnO, (c) the NiO-ZnO heterostructure, (d) absorbance of MB as a function of time.

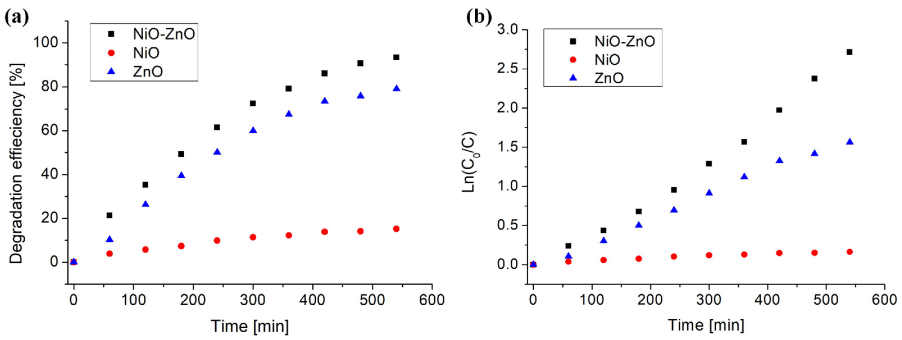

Fig. 7. (a) Degradation efficiency of MB and (b) $\ln(C_0/C)$ curve *vs*. time.

degradation follows a pseudo-first-order kinetic model, described by the equation

$$\ln\left(\frac{C_0}{C}\right) = kt, \tag{3}$$

where k represents the kinetic rate constant (min^{-1}) and t is the irradiation time. The slopes of the curves correspond to the reaction rate constants, indicating that the NiO-ZnO heterostructure exhibits the fastest photodegradation effect [Fig. 7(b)]. The rate constant for the heterostructure was 0.051 min^{-1}, for ZnO 0.031 min^{-1}, and for NiO 0.003 min^{-1}.

In Fig. 8, the photocatalytic mechanism of the NiO-ZnO heterostructure is presented. Under UV irradiation, electron–hole pairs are generated mainly in the ZnO layer. The photogenerated electrons reduce dissolved oxygen to superoxide radicals ($\cdot O_2^-$), while photogenerated holes oxidise water molecules or hydroxide ions to produce hydroxyl radicals ($\cdot OH$). These highly reactive oxygen species attack MB molecules, leading to oxidative degradation rather than direct reduction during photocatalysis. The photogenerated electrons are primarily involved in oxygen reduction, while hydroxyl and superoxide radicals oxidise MB molecules, leading to their stepwise decomposition and mineralisation.

Table 1 summarises selected literature reports on NiO-ZnO heterostructures used for photocatalytic degradation of MB dye. Most studies focus on nanopowders or relatively thick films, which provide a large active surface area but limit material recovery and reusability. In contrast, the present work demonstrates that a thin-film NiO-ZnO heterostructure fabricated by PVD and thermal oxidation achieves high degradation efficiency despite the extremely low catalyst mass, highlighting the potential of thin-film heterostructures for photocatalytic systems. The mass of the NiO-ZnO heterostructure photocatalyst was estimated based on the nominal film thicknesses, substrate area, and bulk density values of the constituent oxides. The mass of photocatalyst (M_{phot}) was calculated using the relation $M_{phot} = \rho \cdot P \cdot d$, where ρ is the material density (for ZnO, it is 5.68 g/cm^3, and for NiO, it is 6.72 g/cm^3), P is the coated substrate area, and d is the film thickness. For a ZnO layer with a thickness of 100 nm and an NiO layer with a thickness of 50 nm deposited on a quartz substrate with an area of 1.68 cm^2, the total photocatalyst mass was estimated to be approximately 0.15 mg. It should be noted that this value represents an upper-limit estimation, as thin films may exhibit reduced effective density due to porosity and grain boundaries. The extremely low catalyst mass highlights the material efficiency of the thin-film heterostructure compared to conventional powder-based photocatalysts, which typically require milligram-scale quantities.

Table 1.
Comparison of photocatalytic performance of materials toward the degradation of MB.

Material form	M_{phot} [mg]	D [%]	Time [min]	MB [mg/L]	Ref.
ZnO/NiO (powder)	50	83	180	32	[45]
NiO-ZnO-Ag (powder)	20	94	90	10	[46]
NiO-ZnO (powder)	75	97	175	7	[47]
ZnO/La_2O_3/NiO (powder)	5	65	150	2	[48]
ZnO (nanowires)	20	100	4320	10	[49]
NiO-ZnO (thin films)	0.15	93	540	5	This work

4. Conclusions

The NiO-ZnO heterostructure was fabricated using a physical vapour deposition followed by thermal oxidation. Structural analyses confirmed the formation of well-crystallised nanograins of NiO and ZnO with distinct cubic and wurtzite phases in the heterostructure.

Despite the catalytic material low mass due to the thin-film configuration, the NiO-ZnO heterostructure demonstrated promising photocatalytic performance, achieving 93% MB degradation after 540 min of irradiation.

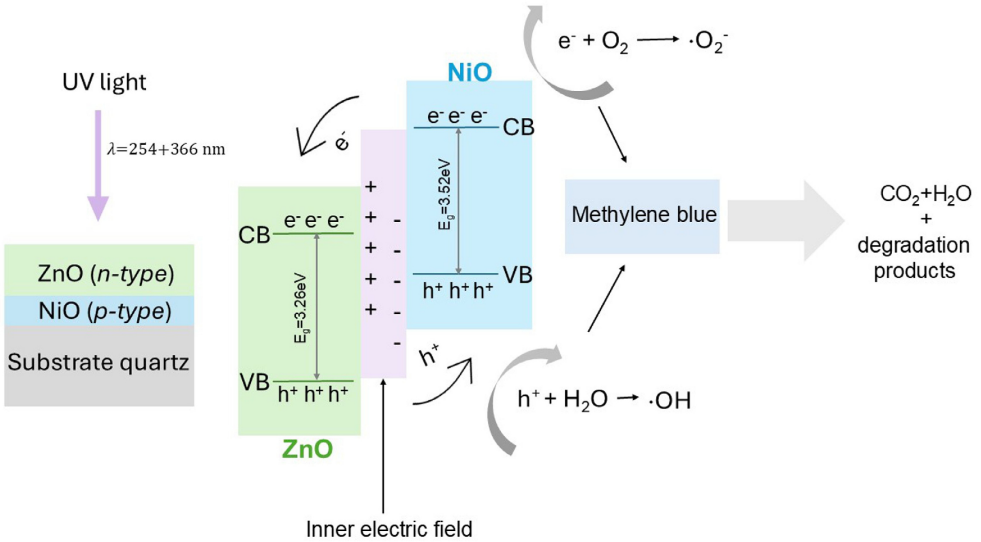

Fig. 8. Schematic illustration of the photocatalytic mechanism of the NiO-ZnO heterostructure under UV irradiation.

These findings indicate that thin-film NiO-ZnO heterostructures can serve as efficient, stable, and easily recoverable photocatalysts. Future work will focus on optimising oxidation conditions, film thickness, and heterojunction architecture to improve visible-light activity and reduce reaction time, extending the applicability of these materials to large-scale water purification systems.

Authors' statement

Research concept and design, I.S., J.R.; collection, data analysis, and interpretation, I.S., J.R., M.K, R.D.; writing the article, I.S.; critical revision of the article, J.R.

Acknowledgements

This research was funded in whole by the National Science Centre of Poland, grant no. 2024/08/X/ST11/00838.

References

[1] Hübner, U. *et al*. Advanced oxidation processes for water and wastewater treatment – Guidance for systematic future research. *Heliyon* **10**, e30402 (2024). https://doi.org/10.1016/j.heliyon.2024.e30402

[2] He, F., Yeon, W. & Choi, W. Photocatalytic air purification mimicking the self-cleaning process of the atmosphere. *Nat. Commun*. **12**, 2528 (2021). https://doi.org/10.1038/s41467-021-22839-0

[3] Wawrzyńczak, A. & Feliczak-Guzik, A. Hydrogen production using modern photocatalysts. *Coatings* **14**, 366 (2024). https://doi.org/10.3390/coatings14030366

[4] Bodzek, M. Nanoparticles for water disinfection by photocatalysis: A review. *Arch. Environ. Prot*. **48**, 3–17 (2022). https://doi.org/10.24425/aep.2022.140541

[5] Braslavsky, S. E. *Glossary of Terms Used in Photochemistry*, *3rd ed.* (IUPAC, 2006). https://doi.org/10.1351/goldbook.P04580

[6] Fujishima, A. & Honda, K. Electrochemical photolysis of water at a semiconductor electrode. *Nature* **238**, 37–38 (1972). https://doi.org/10.1038/238037a0

[7] Guo, Q., Zhou, C., Ma, Z. & Yung, X. Fundamentals of TiO_2 photocatalysis: Concepts, mechanisms, and challenges. *Adv. Mater*. **31**, 1901997 (2019). https://doi.org/10.1002/adma.201901997

[8] Nakata, K. & Fujishima, A. TiO_2 photocatalysis: Design and applications. *J. Photochem. Photobiol. C* **13**, 169–189 (2012). https://doi.org/10.1016/j.jphotochemrev.2012.06.001

[9] Ishibashi, K., Fujishima, A., Watanabe, T. & Hashimoto, K. Quantum yields of active oxidative species formed on TiO_2 photocatalyst. *J. Photochem. Photobiol. A Chem.* **134**, 139–142 (2000). https://doi.org/10.1016/S1010-6030(00)00264-1

[10] Richards, B. S. Comparison of TiO_2 and other dielectric coatings for buried-contact solar cells: A review. *Prog. Photovolt*. **12**, 253–281 (2004). https://doi.org/10.1002/pip.529

[11] Khodja, A. A., Sehili, T., Pilichowski, J.-P. & Boule, P. Photocatalytic degradation of 2-phenylphenol on TiO_2 and ZnO in aqueous suspensions. *J. Photochem. Photobiol. A Chem.* **141**, 231–239 (2001). https://doi.org/10.1016/S1010-6030(01)00423-3

[12] Chakrabarti, S. & Dutta, B. K. Photocatalytic degradation of model textile dyes in wastewater using ZnO as semiconductor catalyst. *J. Hazard. Mater.* **112**, 269–278 (2004). https://doi.org/10.1016/j.jhazmat.2004.05.013

[13] Lin, H., Liao, S.-C. & Hung, S.-W. The dc thermal plasma synthesis of ZnO nanoparticles for visible-light photocatalyst. *J. Photochem. Photobiol. A Chem.* **174**, 82–87 (2005). https://doi.org/10.1016/j.jphotochem.2005.02.015

[14] Sakthivel, S. *et al*. Solar photocatalytic degradation of azo dye: comparison of photocatalytic efficiency of ZnO and TiO_2. *Sol. Energy Mater. Sol. Cells* **77**, 65–82 (2003). https://doi.org/10.1016/S0927-0248(02)00255-6

[15] Gurushantha, K. *et al*. New green synthesized reduced graphene oxide–ZrO_2 composite as high performance photocatalyst under sunlight. *RSC Adv*. **7**, 12690–12703 (2017). https://doi.org/10.1039/C6RA25823A

[16] Hitam, C. & Jalil, A. A review on Fe_2O_3 photocatalyst towards degradation of dyes and organic contaminants. *J. Environ. Manag*. **258**, 110050 (2020). https://doi.org/10.1016/j.jenvman.2019.110050

[17] Adhikari, S., Chandra, K. S., Kim, D.-H., Madras, G. & Sarkar, D. Understanding the morphological effects of WO_3 photocatalysts for the degradation of organic pollutants. *Adv. Powder Technol*. **29**, 1591–1600 (2018). https://doi.org/10.1016/j.apt.2018.03.024

[18] Kusmierek, E. A CeO_2 semiconductor as a photocatalytic and photoelectrocatalytic material for the remediation of pollutants in industrial wastewater: A Review. *Catalysts* **10**, 1435 (2020). https://doi.org/10.3390/catal10121435

[19] Sajid, M. M. *et al*. Preparation and characterization of vanadium pentoxide (V_2O_5) for photocatalytic degradation of monoazo and diazo dyes. *Surf. Interfaces* **19**, 100502 (2020). https://doi.org/10.1016/j.surfin.2020.100502

[20] Ye, Z. *et al*. A comparative photocatalytic activity of ZnS photocatalyst for degradation of various dyes. *Optik* **164**, 345–354 (2018). https://doi.org/10.1016/j.ijleo.2018.03.030

[21] Zhong, Y., Zhao, G., Ma, F., Wu, Y. & Hao, Y. Utilizing photocorrosion-recrystallization to prepare a highly stable and efficient CdS/WS_2 nanocomposite photocatalyst for hydrogen evolution. *Appl. Catal. B: Environ.* **199**, 466–472 (2016). https://doi.org/10.1016/j.apcatb.2016.06.065

[22] Xiang, Q., Chen, F. & Lang. D. Hierarchical WS_2/graphene-modified CdS nanorods for efficient photocatalytic hydrogen evolution. *ChemSusChem* **9**, 996–1002 (2016). https://doi.org/10.1002/cssc.201501702

[23] Murakami, S.-Y. *et al*. Evaluation of electron–hole recombination properties of titanium (IV) oxide particles with high photocatalytic activity. *Res. Chem. Intermed*. **33**, 285–296 (2007). https://doi.org/10.1163/156856707779238612

[24] Zhu, D. & Zhou, Q. Action and mechanism of semiconductor photocatalysis on degradation of organic pollutants in water treatment: A review. *Environ. Nanotechnol. Monit. Manag*. **12**, 100255 (2019). https://doi.org/10.1016/j.enmm.2019.100255

[25] Seo, Y. S. & Oh, S. G. Controlling the recombination of electron-hole pairs by changing the shape of ZnO nanorods via sol-gel method using water and their enhanced photocatalytic properties. *Korean J. Chem. Eng*. **36**, 2118–2124 (2019). https://doi.org/10.1007/s11814-019-0401-0

[26] Hosny, N. M., Gomaa, I., Elmahgary, M. G. & Ibrahim, M. A. ZnO doped C: Facile synthesis, characterization and photocatalytic degradation of dyes. *Sci. Rep.* **13**, 14173 (2023). https://doi.org/10.1038/s41598-023-41106-4

[27] Hussain, A., Fiaz, S., Almohammedi, A. & Waqar, A. Optimizing photocatalytic performance with Ag-doped ZnO nanoparticles: Synthesis and characterization. *Heliyon* **10**, e35725 (2024). https://doi.org/10.1016/j.heliyon.2024.e35725

[28] Tong, T., Zhang, J., Tian, B., Chen, F. & He, D. Preparation of Fe^{3+}-doped TiO_2 catalysts by controlled hydrolysis of titanium alkoxide and study on their photocatalytic activity for methyl orange degradation. *J. Hazard. Mater*. **155**, 572–579 (2008). https://10.1016/j.jhazmat.2007.11.106

[29] Nada, E. A. *et al*. Enhanced photocatalytic activity of WS_2/TiO_2 nanofibers for degradation of phenol under visible light irradiation. *Inorganics* **10**, 54 (2022). https://doi.org/10.3390/inorganics10040054

[30] Ding, J. *et al*. Distinctly different active sites of ZnO–ZrO_2 catalysts in CO_2 and CO hydrogenation to methanol reactions. *Nat. Commun*. **16**, 4622 (2025). https://doi.org/10.1038/s41467-025-59996-5

[31] Rashid, H. *et al*. Synthesis, structural and photocatalytic properties of ZnO-CuO, ZnO-graphene and ZnO-CuO-graphene nanocomposites. *Polyhedron* **273**, 117471 (2025). https://doi.org/10.1016/j.poly.2025.117471

[32] Shi, M. *et al*. Temperature-controlled crystal size of wide band gap NiO and its application in electrochromism. *Micromachines* **12**, 80 (2021). https://doi.org/10.3390/mi12010080

[33] Rymarczyk, J. & Stępińska, I. CuO-ZnO nanocomposite for photocatalytic applications. *J. Vac. Sci. Technol. B* **42**, 032801 (2024). https://doi.org/10.1116/6.0003482

[34] Ma, M. J. *et al*. Orientation dependent band alignment for *p*-NiO/*n*-ZnO heterojunctions. *J. Appl. Phys.* **113**, 163704 (2013). https://doi.org/10.1063/1.4803095

[35] Saeed, M. *et al*. Synthesis of p-n NiO-ZnO heterojunction for photodegradation of crystal violet dye. *Alex. Eng. J.* **65**, 561–574 (2023). https://doi.org/10.1016/j.aej.2022.09.048

[36] Gasmi, M., Djelloul, A., Iaiche, S., Lahouel, K. & Baydogan, L. Excellent photocatalytic activity of ZnO-NiO heterojunction thin film in the sunlight range with enhanced of UV photodetection behavior. *J. Sol-Gel Sci. Technol.* **114**, 699–717 (2025). https://doi.org/10.1007/s10971-025-06728-2

[37] Faris, N. H. Q. & Aljarrah, R. M. Employ ZnO/NiO nanocomposites as catalyst for photo degradation of methylene orange dye in water. *J. Nano Mater. Impact* **1**, 10–16 (2025). https://doi.org/10.71109/nmi.2025.1.2.11

[38] Arun, V. *et al*. Synthesis and photocatalytic performance of ZnO/NiO-decorated reduced graphene oxide nanohybrids for methylene blue degradation. *Ionics* **31**, 4705–4723 (2025). https://doi.org/10.1007/s11581-025-06220-5

[39] Chu, Y.-L., Liu, Y.-H, Chu, T.-T. & Young, S.-J. Improved UV-sensing of Au-decorated ZnO nanostructure MSM photodetectors. *IEEE Sens. J.* **22**, 5644–5650 (2022). https://doi.org/10.1109/JSEN.2022.3150254

[40] Tan, G. *et al*. ZnO@NiO core-shell heterojunction photoanode with NiOOH co-catalyst for high-performance self-powered photoelectrochemical-type UV photodetector. *Appl. Surf. Sci*. **681**, 161579 (2025). https://doi.org/10.1016/j.apsusc.2024.161579

[41] Patil, S. & Kadam, L. D. Preparation and characterization of spray pyrolyzed nickel oxide (NiO) thin films *Appl. Surf. Sci*. **199**, 211–221 (2002). https://doi.org/10.1016/S0169-4332(02)00839-5

[42] Dejam, L. *et al*. Advanced nano-texture, optical band gap, and Urbach energy analysis of NiO/Si heterojunctions. *Sci. Rep.* **13**, 6518 (2023). https://doi.org/10.1038/s41598-023-33713-y

[43] Sharma, S., Periasamy, C. & Chakrabarti, P. Thickness dependent study of RF sputtered ZnO thin films for optoelectronic device applications. *Electron. Mater. Lett.* **11**, 1093–1101 (2015). https://doi.org/10.1007/s13391-015-4445-y

[44] Tan, S. T. *et al*. Blueshift of optical band gap in ZnO thin films grown by metal-organic chemical-vapor deposition. *J. Appl. Phys.* **98**, 013505 (2005). https://doi.org/10.1063/1.1940137

[45] Karthikeyan, V. *et al*. Synthesis and characterization of ZnO/NiO and its photocatalytic activity. *Mech. Mater. Sci. Eng*. **9**, 1–8 (2017). https://hal.archives-ouvertes.fr/hal-01499366/file/ID2017022242.pdf

[46] Aydoghmish, S. M., Hassanzadeh-Tabrizi, S. A. & Saffar-Teluri, A. Facile synthesis and investigation of NiO–ZnO–Ag nanocomposites as efficient photocatalysts for degradation of methylene blue dye. *Ceram. Int.* **45**, 14934–14942 (2019). https://doi.org/10.1016/j.ceramint.2019.04.229

[47] Weldekirstos, H. D., Habtewold, B. & Kabtamu, D. M. Surfactant-assisted synthesis of NiO-ZnO and NiO-CuO nanocomposites for enhanced photocatalytic degradation of methylene blue under UV light irradiation. *Front. Mater.* **9**, 832439 (2022). https://doi.org/10.3389/fmats.2022.832439

[48] Shubha, J. P. *et al*. ZnO/La_2O_3/NiO based ternary heterostructure nano-photocatalyst: Preparation, characterization and its application for the degradation of methylene blue. *J. King Saud Univ. Sci.* **34**, 101738 (2022). https://doi.org/10.1016/j.jksus.2021.101738

[49] Mahana, A., Guliy, Y., Momin, S. C., Lalmuanzeli, R. & Mehta, S. H. Sunlight-driven photocatalytic degradation of methylene blue using ZnO nanowires prepared through ultrasonication-assisted biological process using aqueous extract of *Anabaena doliolum*. *Opt. Mater.* **108**, 110205 (2020). https://doi.org/10.1016/j.optmat.2020.110205